Atomic Diffusion of Indium through Threading Dislocations in InGaN Quantum Wells

Yudai Yamaguchi,[*,†] *Yuya Kanitani,*[†] *Yoshihiro Kudo,*[†] *Jun Uzuhashi,*[‡] *Tadakatsu Ohkubo,*[‡] *Kazuhiro Hono*[‡] *and Shigetaka Tomiya*[*,†]

[†] R&D Center, Sony Group Corporation, 4-14-1 Asahi-cho, Atsugi, Kanagawa 243-0014, Japan

[‡] National Institute for Materials Science, 1-2-1 Sengen, Tsukuba, Ibaraki 305-0047, Japan

The compositional and structural investigations of threading dislocations (TDs) in InGaN/GaN multiple quantum wells were carried out using correlative transmission electron microscopy (TEM) and atom probe tomography (APT). The correlative TEM/APT analysis on the same TD reveals that the indium atoms are diffused along the TD and its concentration decreases with distance from the InGaN layer. Based on the results, we directly observed that the indium atoms originating from the InGaN layer diffuse toward the epitaxial GaN surface through the TD, and it is considered to have occurred via the pipe diffusion mechanism induced by strain energy relaxation.

Keywords: Dislocation, InGaN, pipe diffusion, atom probe tomography, transmission electron microscopy

Group III nitride semiconductors such as GaN are currently being considered promising candidates for applications in various fields such as optoelectronics, photovoltaics, and power electronics. For example, mixed crystals of GaN, InN, and AlN can be used in devices such as light emitting diodes (LEDs),[1,2] laser diodes (LDs),[3] solar cells,[4] and high electron mobility transistors (HEMTs)[5–7] owing to the ease of tuning the band gap by changing their mixing ratio.

Group III nitride semiconductors are often grown on GaN, sapphire, SiC, and Si substrates. However, when these heterosubstrates are used, threading dislocations (TDs) with a number density of from 10^8 to 10^{10} cm^{-2} are undesirably formed during epitaxial growth because of the differences between the lattice constants of the substrate and growing layer.[8–12] These dislocations have been reported to result in the loss of key characteristics in devices such as light-emitting devices,[13–15] solar cells,[16] and HEMTs.[17] The electronic state of the dislocations changes by the local structure and composition near the dislocation core;[18–20] therefore, it is crucial to understand these structure-property relationships to improve the characteristics of these devices.

To date, there have been many studies of the relationship between dislocations and composition in mixed crystals of group III nitride semiconductors,[21–29] and it is known that a local strain field is formed around dislocations, and the compositional changes occur in mixed crystals such as InGaN,[21–24] AlGaN,[24–26] and AlInN.[18, 27, 28] Massabuau *et al.* reported that such compositional deviations can cause carrier localization in the locality of the dislocation.[29] In these previous studies, transmission electron microscopy (TEM) and scanning transmission electron microscopy (STEM) were used for the structural and compositional analysis of dislocations. However, these analytical (S-)TEM techniques are two-dimensional (2D) in principle, so information on the elemental distribution is averaged through (S-)TEM specimens.

Therefore, an atomic-scale three-dimensional (3D) analytical method is required to reveal the elemental distribution around the dislocation in detail.

Atom probe tomography (APT) has a high spatial resolution (on the subnanometer scale) and a relatively low detection limit, making it an ideal technique for the evaluation of the local distribution of trace elements near crystal defects such as dislocations and V-pits.[30–39] In contrast, (S-)TEM are suitable for providing crystal information; that is, the analysis of the Burgers vector of dislocations, as well as for obtaining details of the structure of the core. In this study, we investigated the elemental distribution around TDs penetrating InGaN/GaN multiple quantum wells (MQWs) using the correlative TEM and APT analysis.

First, an InGaN MQW film was grown on a sapphire (0001) substrate. The film consisted of a 5.4-μm-thick GaN layer, four pairs of 3-nm-thick $In_xGa_{1-x}N$ QW layers, and 10-nm-thick GaN layers having different indium compositions (x = 0.08, 0.15, 0.25, and 0.35 from bottom to top), that is, GaN (5.4 μm)/[$In_xGa_{1-x}N$ (3 nm)/GaN (10 nm)]$_4$, and, finally, an additional 140-nm-thick GaN cap layer grown as the top layer.

The needle-shaped specimen for the correlative TEM and APT analysis was prepared by the lift-out method from the grown sample onto a TEM grid using focused ion beam-scanning electron microscopy (FIB-SEM, Helios G4UX, ThermoFisher). The specimen, which contained one TD, was fabricated into the needle shape using annular FIB milling. Then, the needle-shaped specimen was cleaned at 2 kV to reduce the damage caused by the high-energy Ga ion beam. The APT measurements were performed using a local electrode atom probe (LEAP5000XS, AMETEK) under 250-kHz pulsed UV laser excitation (355 nm) at a specimen temperature of 30

K in an ultrahigh vacuum. A laser pulse energy of 100 fJ was selected. For visualization and analysis, IVAS (version 3.8.8) was used to produce 3D atom maps of the specimen.

Before the APT measurements, the bright field (BF)-TEM observation was performed to confirm the shape and structure of the specimen, as well as weak-beam dark-field (WBDF)-TEM to analyze the Burgers vector of the TD in the specimen. The TEM analysis was performed in a JEOL JEM2000FX-II at 200 kV. Then the APT measurement was performed followed by the plan-view high-angle annular dark field (HAADF)-STEM observation on the needle-shaped specimen. APT is a destructive analytical technique and the InGaN layer is completely ionized by APT measurement; thus, the dislocation core in the InGaN layer cannot be observed directly. Therefore, the structure of the dislocation core in the GaN layer left in the needle-shaped specimen was observed. The specimen for plan-view analysis was prepared as follows: the needle-shaped specimen after the APT measurement was transferred to another TEM grid by FIB-SEM and thinned along the [0001] direction at 30 kV. Finally, Ar-ion milling was performed at 350 V using a TECHNOORG-Linda Gentle Mill to reduce Ga ion beam damage. Subsequently, HAADF-STEM plan-view observation was performed in a JEOL ARM-300F at 300 kV. The acquisition angles of the HAADF detector ranged from 45–180 mrad.

Figure 1a shows a SEM image of the sample surface. The orange rectangle in Figure 1a indicates the region where the needle-shaped specimen for the TEM/APT analysis was prepared. Figure 1b shows the BF-TEM image of the needle-shaped specimen before the APT measurement. As indicated by the white arrow, the TD can be seen at the center of the needle-shaped specimen.

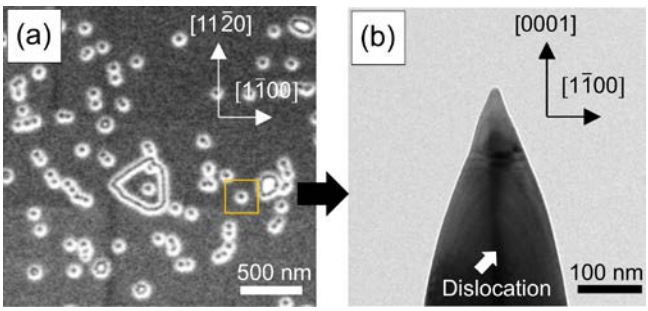

Figure 1. (a) SEM image of the sample surface. The orange rectangle indicates the region where the needle-shaped specimen for TEM/APT was prepared. (b) BF-TEM image of the needle-shaped specimen.

The WBDF-TEM images of the needle-shaped specimen before APT measurements are shown in Figure 2a (***g*** = [3$\bar{3}$00]) and Figure 2b (***g*** = [0004]). In Figure 2a (***g*** = [3$\bar{3}$00]), the bright line contrast at the center of the needle-shaped specimen indicates the TD. In contrast, in Figure 2b (***g*** = [0004]), the contrast corresponding to the TD is no longer visible. This result indicates that the needle-shaped specimen contains an *a*-type dislocation. Figure 2c shows the 3D atom map of the indium atoms obtained from the APT measurements, and Figure 2d shows the same image with iso-concentration-surfaces at 0.4 at.% indium concentration. The indium concentration was calculated by [In counts]/[Ga counts + In counts]. For better visualization of the indium distribution near the TD, 10-nm-thick slices in the *y*-direction are shown in Figures 2c and 2d. As shown in Figure 2c, wells are deformed into a V-shape, thus forming a V-pit (denoted V-shaped wells 1–4 from bottom to top). The indium concentration at the normal well regions (without the V-shaped well), facet regions of the V-shaped well, and bottom regions of the V-shaped wells were calculated by sampling 2 nm cubic in these regions, and Table 1 summarizes the corresponding indium concentrations (see Figure S1 in the Supporting Information for more details). As shown in Table 1, the facet regions of the V-shaped wells have a lower indium

concentration compared to the normal well, whereas the bottom regions have a higher indium concentration. As shown in 2d, the indium atoms are distributed along the TD passing through the center of the V-shaped well. Further, indium atoms are distributed toward the surface direction but not in the substrate direction.

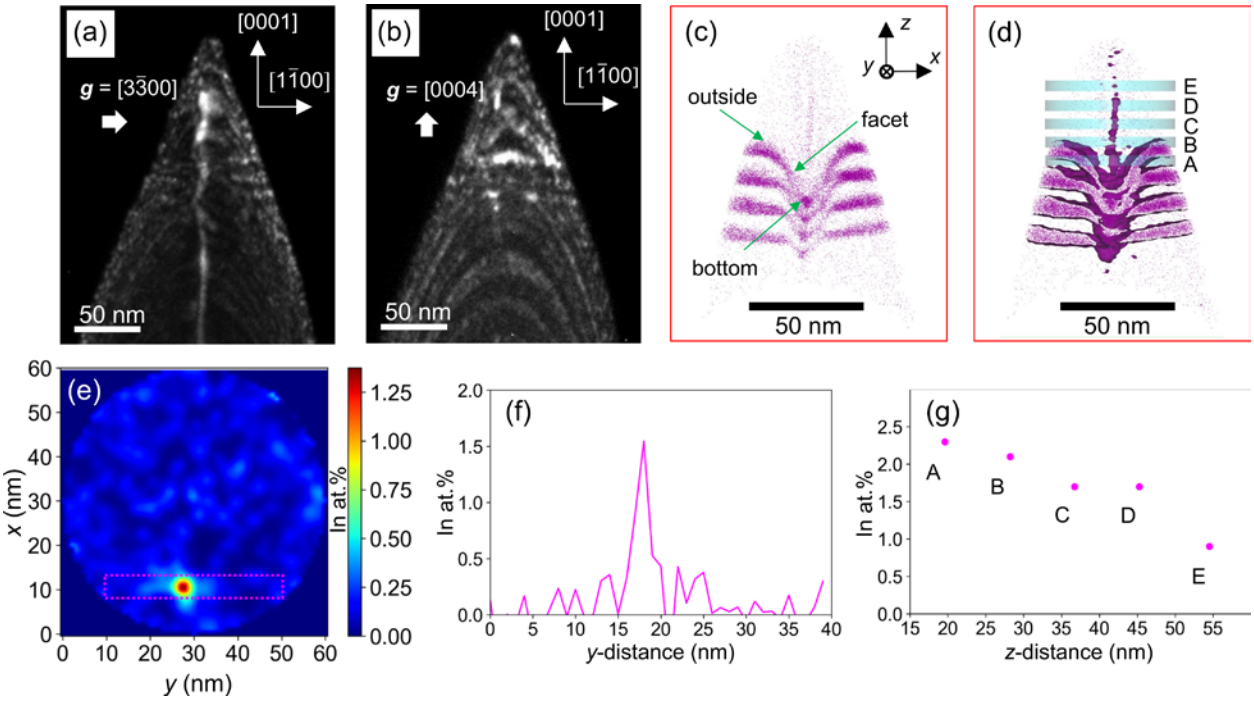

Figure 2. WBDF-TEM images of a needle-shaped specimen with (a) $\boldsymbol{g}$ = [3$\bar{3}$00] and (b) $\boldsymbol{g}$ = [0004]. (c) 3D atom map of the indium obtained from the APT measurements and (d) the same image with iso-concentration-surfaces for [In] = 0.4% (σ = 1.0). Both for (c) and (d), 3D atom maps are sliced with 10-nm thickness in the *y*-direction for better visualization. (e) 2D concentration map of the indium in the crystal growth plane marked region C in (d). (f) Line concentration profile of indium along the region indicated by the dotted line in (e). (g) Relationship between the indium concentration at the dislocation and the distance from the bottom of the fourth V-shaped well. The symbols in the figure correspond to regions A–E in (d).

Table 1. Indium Concentration Around the V-shaped Well (Details of These Values Are Described in Figure S1).

Well number	Outside of V-shaped well	Facet of V-shaped well	Bottom of V-shaped well
4	26.0%	9.3%	44.9%
3	17.8%	8.4%	29.3%
2	9.1%	3.1%	21.4%
1	4.3%	1.0%	12.2%

Figure 2e shows a 2D integrated concentration map of the indium with a thickness of 5 nm in the crystal growth direction (z-direction) of region C (blue frame in Figure 2d). Figure 2f shows the indium concentration profile along the region indicated by the dotted line in Figure 2e, revealing that the indium atoms are present at approximately 1 at.% concentration along the TD in the GaN layer even 37 nm away from the InGaN layer. Figure 2g shows the correlation between the concentration of indium atoms distributed along the TD and the distance from the bottom of the fourth V-shaped well. The symbols A–E in the figure correspond to the labeled regions in Figure 2d. Figure 2g shows that the concentration of indium at the TD gradually decreases as the distance from the InGaN layer increases.

Figure 3a shows the WBDF-TEM image of the needle-shaped specimen after the APT measurement with $\boldsymbol{g} = [3\bar{3}00]$. As shown in Figure 3a, the needle-shaped specimen after the APT measurement also contains the TD. Figures 3b, 3c, and 3d show a plan-view HAADF-STEM image obtained from the region marked by a pink line in Figure 3a, a magnified image of the

dislocation core region, and an image of the dislocation core overlaid with lattice position guides, respectively. Typically, there are three types of core structures in edge dislocations in group III nitrides on the (0001) plane: 8-atom ring, 5/7-atom ring, and 4-atom ring.[40] Figure 3d shows that the dislocation observed in this study is an *a*-type edge dislocation having a 4-atom ring core structure.[40]

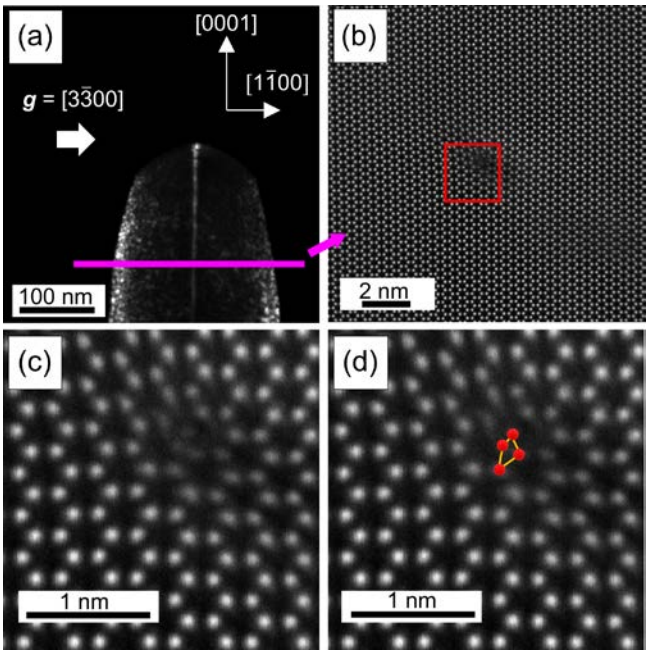

Figure 3. (a) WBDF-TEM image with ***g*** = [3$\bar{3}$00] in the needle-shaped specimen after APT measurement. (b) Plan-view HAADF-STEM image obtained from the region marked by a pink line in (a). (c) Magnified image of the dislocation core shown in the red rectangle in (b). (d) STEM image of the dislocation core overlaid with lattice position guides.

Here, we move to discussions on three issues that are revealed by the correlative TEM/APT analysis: namely, the formation mechanism of the region having a high indium concentration at the bottom of the V-shaped well, the distribution of indium atoms along the TD, and the

direction of the indium distribution. As they are closely related to each other, we discuss them in order along the crystal growth process.

Firstly, we discuss the formation mechanism of the region having a high indium concentration at the bottom of the V-shaped well. As shown by the data in Table 1, the indium concentration at the facet of the V-pit is low, so some of the indium atoms supplied to this region may have diffused along the facet and become incorporated near the edge-dislocation core. Typically, indium segregation occurs around dislocations as a result of the strong tensile strain originating from the edge dislocation,[24, 28] and this phenomenon could be operative at the bottom of the V-pit penetrated by the dislocation.

Secondly, we discuss the distribution of indium atoms along the dislocation. As shown in Figure 2g, the indium concentration distributed near the dislocation in the GaN layer decreases as the distance from the InGaN layer increases: this phenomenon is regarded as resulting from the diffusion of indium atoms from the InGaN layer. Crucially, the diffusion coefficients of the elements present along the dislocation are orders of magnitude larger than those in the defect-free bulk region,[41] and this type of dislocation-induced diffusion has been observed in several materials, including metals such as Al[41] and semiconductors such as InGaAs[35] and Ge.[38, 39] This is known as “pipe diffusion,” and the observed diffusion of elements could be related to this phenomenon. Generally, the driving force for diffusion is a concentration gradient. Thus, indium segregation at the dislocation core enhances its diffusivity.

Finally, we discuss the direction of pipe diffusion. Garbrecht *et al.* reported that strain energy can drive diffusion.[42] Specifically, indium atoms in the high indium concentration region preferentially diffuse to the surface side along the dislocation to achieve strain relaxation at the

surface (bottom of the V-pit). Thus, using the strain energy, we can explain why the direction of diffusion of the indium atoms is restricted toward the surface: The pipe diffusion of indium atoms is driven by both the indium concentration gradient and the strain energy. Further, since the GaN layer is formed at a higher temperature than the InGaN layer immediately below it, the thermal energy may accelerate pipe diffusion.

In summary, a detailed compositional and structural analysis of the TD through an InGaN/GaN MQW was carried out using the correlative TEM/APT technique. Based on the results, we observed that the pipe diffusion of indium atoms occurred through edge dislocation. Furthermore, we conclude that the gradient in the indium concentration at the bottom of the V-shaped well and the strain energy could be the driving force behind the observed pipe diffusion. By applying our developed correlative TEM/APT analysis, we are investigating the edge dislocations in other group III nitride semiconductor mixed crystals such as AlInN and AlGaN, as well as other types of dislocations. These investigations would be a crucial key to improving the property of group III nitride semiconductor-based devices.

ASSOCIATED CONTENT

Supporting Information

Additional information including the regions used to calculate the indium concentration at each position in the wells (as well as the nomenclature, *i.e.*, the normal well, facet of the V-shaped well, and bottom regions).

AUTHOR INFORMATION

Corresponding Author

*Yudai Yamaguchi

E-mail: Yudai.Yamaguchi@sony.com

*Shigetaka Tomiya

E-mail: Shigetaka.Tomiya@sony.com

REFERENCES

(1) Nakamura, S.; Senoh, M.; Iwasa, N.; Nagahama, S. I. High-Brightness InGaN Blue, Green and Yellow Light-Emitting Diodes with Quantum Well Structures. *Jpn. J. Appl. Phys.* **1995**, *34* (7), L797–L799. https://doi.org/10.1143/JJAP.34.L797.

(2) Mukai, T.; Yamada, M.; Nakamura, S. Characteristics of InGaN-Based UV/Blue/Green/Amber/Red Light-Emitting Diodes. *Japanese J. Appl. Physics, Part 1 Regul. Pap. Short Notes Rev. Pap.* **1999**, *38* (7 B), 3976–3981. https://doi.org/10.1143/jjap.38.3976.

(3) Nakamura, S. The Roles of Structural Imperfections in InGaN-Based Blue Light- Emitting Diodes and Laser Diodes. *Science (80-.).* **1998**, *281* (5379), 956–961. https://doi.org/10.1126/science.281.5379.956.

(4) Jani, O.; Ferguson, I.; Honsberg, C.; Kurtz, S. Design and Characterization of GaN/InGaN Solar Cells. *Appl. Phys. Lett.* **2007**, *91* (13), 132117. https://doi.org/10.1063/1.2793180.

(5) Asif Khan, M.; Bhattarai, A.; Kuznia, J. N.; Olson, D. T. High Electron Mobility Transistor Based on a GaN-$Al_xGa_{1-x}N$ Heterojunction. *Appl. Phys. Lett.* **1993**, *63* (9), 1214–1215. https://doi.org/10.1063/1.109775.

(6) Gonschorek, M.; Carlin, J. F.; Feltin, E.; Py, M. A.; Grandjean, N.; Darakchieva, V.; Monemar, B.; Lorenz, M.; Ramm, G. Two-Dimensional Electron Gas Density in $Al_{1-x}In_xN$/AlN/GaN Heterostructures ($0.03 \leq x \leq 0.23$). *J. Appl. Phys.* **2008**, *103* (9), 93714. https://doi.org/10.1063/1.2917290.

(7) Baliga, B. J. Gallium Nitride Devices for Power Electronic Applications. *Semicond. Sci. Technol.* **2013**, *28* (7), 74011. https://doi.org/10.1088/0268-1242/28/7/074011.

(8) Lester, S. D.; Ponce, F. A.; Craford, M. G.; Steigerwald, D. A. High Dislocation Densities in High Efficiency GaN-Based Light-Emitting Diodes. *Appl. Phys. Lett.* **1995**, *66* (10), 1249. https://doi.org/10.1063/1.113252.

(9) Rhode, S. K.; Horton, M. K.; Kappers, M. J.; Zhang, S.; Humphreys, C. J.; Dusane, R. O.; Sahonta, S. L.; Moram, M. A. Mg Doping Affects Dislocation Core Structures in GaN. *Phys. Rev. Lett.* **2013**, *111* (2). https://doi.org/10.1103/PhysRevLett.111.025502.

(10) Sakai, S.; Wang, T.; Morishima, Y.; Naoi, Y. New Method of Reducing Dislocation Density in GaN Layer Grown on Sapphire Substrate by MOVPE. *J. Cryst. Growth* **2000**, *221* (1–4), 334–337. https://doi.org/10.1016/S0022-0248(00)00709-0.

(11) Marchand, H.; Zhao, L.; Zhang, N.; Moran, B.; Coffie, R.; Mishra, U. K.; Speck, J. S.; DenBaars, S. P.; Freitas, J. A. Metalorganic Chemical Vapor Deposition of GaN on Si(111): Stress Control and Application to Field-Effect Transistors. *J. Appl. Phys.* **2001**, *89* (12), 7846–7851. https://doi.org/10.1063/1.1372160.

(12) Inoki, C. K.; Kuan, T. S.; Lee, C. D.; Sagar, A.; Feenstra, R. M.; Koleske, D. D.; Díaz, D. J.; Bohn, P. W.; Adesida, I. Growth of GaN on Porous SiC and GaN Substrates. *J. Electron. Mater.* **2003**, *32* (8), 855–860. https://doi.org/10.1007/s11664-003-0200-5.

(13) Schubert, M. F.; Chhajed, S.; Kim, J. K.; Schubert, E. F.; Koleske, D. D.; Crawford, M. H.; Lee, S. R.; Fischer, A. J.; Thaler, G.; Banas, M. A. Effect of Dislocation Density on Efficiency Droop in GaInN/GaN Light-Emitting Diodes. *Appl. Phys. Lett.* **2007**, *91* (23), 231114. https://doi.org/10.1063/1.2822442.

(14) Sugahara, T.; Sato, H.; Hao, M.; Naoi, Y.; Kurai, S.; Tottori, S.; Yamashita, K.; Nishino, K.; Romano, L. T.; Sakai, S. Direct Evidence That Dislocations Are Non-Radiative Recombination Centers in GaN. *Jpn. J. Appl. Phys.* **1998**, *37* (4A), L398–L400. https://doi.org/10.1143/jjap.37.l398.

(15) Chernyakov, A. E.; Sobolev, M. M.; Ratnikov, V. V.; Shmidt, N. M.; Yakimov, E. B. Nonradiative Recombination Dynamics in InGaN/GaN LED Defect System. *Superlattices Microstruct.* **2009**, *45* (4–5), 301–307. https://doi.org/10.1016/j.spmi.2008.10.045.

(16) Zhang, Y.; Kappers, M. J.; Zhu, D.; Oehler, F.; Gao, F.; Humphreys, C. J. The Effect of Dislocations on the Efficiency of InGaN/GaN Solar Cells. *Sol. Energy Mater. Sol. Cells* **2013**, *117*, 279–284. https://doi.org/10.1016/j.solmat.2013.06.022.

(17) Tapajna, M.; Kaun, S. W.; Wong, M. H.; Gao, F.; Palacios, T.; Mishra, U. K.; Speck, J. S.; Kuball, M. Influence of Threading Dislocation Density on Early Degradation in AlGaN/GaN High Electron Mobility Transistors. *Appl. Phys. Lett.* **2011**, *99* (22), 223501. https://doi.org/10.1063/1.3663573.

(18) Kioseoglou, J.; Kalesaki, E.; Belabbas, I.; Chen, J.; Nouet, G.; Kirmse, H.; Neumann, W.; Komninou, P.; Karakostas, T. Screw Threading Dislocations in AlN: Structural and Electronic Properties of In and O Doped Material. *J. Appl. Phys.* **2011**, *110* (5), 53715. https://doi.org/10.1063/1.3632985.

(19) Belabbas, I.; Chen, J.; Nouet, G. Electronic Structure and Metallization Effects at Threading Dislocation Cores in GaN. *Comput. Mater. Sci.* **2014**, *90*, 71–81. https://doi.org/10.1016/j.commatsci.2014.04.021.

(20) Takei, Y.; Nakayama, T. Electron-Carrier Generation by Edge Dislocations in InN Films: First-Principles Study. *J. Cryst. Growth* **2009**, *311* (10), 2767–2771. https://doi.org/10.1016/j.jcrysgro.2009.01.019.

(21) Horton, M. K.; Rhode, S.; Sahonta, S. L.; Kappers, M. J.; Haigh, S. J.; Pennycook, T. J.; Humphreys, C. J.; Dusane, R. O.; Moram, M. A. Segregation of In to Dislocations in InGaN. *Nano Lett.* **2015**, *15* (2), 923–930. https://doi.org/10.1021/nl5036513.

(22) Lei, H.; Chen, J.; Ruterana, P. Influences of the Biaxial Strain and *c*-Screw Dislocation on the Clustering in InGaN Alloys. *J. Appl. Phys.* **2010**, *108* (10), 103503. https://doi.org/10.1063/1.3509147.

(23) Rhode, S. L.; Horton, M. K.; Sahonta, S. L.; Kappers, M. J.; Haigh, S. J.; Pennycook, T. J.; McAleese, C.; Humphreys, C. J.; Dusane, R. O.; Moram, M. A. Dislocation Core Structures in (0001) InGaN. *J. Appl. Phys.* **2016**, *119* (10), 105301. https://doi.org/10.1063/1.4942847.

(24) Sakaguchi, R.; Akiyama, T.; Nakamura, K.; Ito, T. Theoretical Investigations of Compositional Inhomogeneity Around Threading Dislocations in III-Nitride Semiconductor Alloys. *Jpn. J. Appl. Phys.* **2016**, *55* (5), 05FM05. https://doi.org/10.7567/JJAP.55.05FM05.

(25) Chang, L.; Lai, S. K.; Chen, F. R.; Kai, J. J. Observations of Al Segregation Around Dislocations in AlGaN. *Appl. Phys. Lett.* **2001**, *79* (7), 928–930. https://doi.org/10.1063/1.1391409.

(26) Massabuau, F. C. P.; Rhode, S. L.; Horton, M. K.; O'Hanlon, T. J.; Kovács, A.; Zielinski, M. S.; Kappers, M. J.; Dunin-Borkowski, R. E.; Humphreys, C. J.; Oliver, R. A. Dislocations in AlGaN: Core Structure, Atom Segregation, and Optical Properties. *Nano Lett.* **2017**, *17* (8), 4846–4852. https://doi.org/10.1021/acs.nanolett.7b01697.

(27) Lei, H.; Chen, J.; Ruterana, P. Role of c -Screw Dislocations on Indium Segregation in InGaN and InAlN Alloys. *Appl. Phys. Lett.* **2010**, *96* (16), 161901. https://doi.org/10.1063/1.3394007.

(28) Mouti, A.; Rouvière, J. L.; Cantoni, M.; Carlin, J. F.; Feltin, E.; Grandjean, N.; Stadelmann, P. Stress-Modulated Composition in the Vicinity of Dislocations in Nearly Lattice Matched $Al_xIn_{1-x}N$/GaN Heterostructures: A Possible Explanation of Defect Insensitivity. *Phys. Rev. B - Condens. Matter Mater. Phys.* **2011**, *83* (19). https://doi.org/10.1103/PhysRevB.83.195309.

(29) Massabuau, F. C. P.; Chen, P.; Horton, M. K.; Rhode, S. L.; Ren, C. X.; O'Hanlon, T. J.; Kovács, A.; Kappers, M. J.; Humphreys, C. J.; Dunin-Borkowski, R. E.; et al. Carrier Localization in the Vicinity of Dislocations in InGaN. *J. Appl. Phys.* **2017**, *121* (1), 13104. https://doi.org/10.1063/1.4973278.

(30) Blavette, D.; Cadel, E.; Fraczkiewicz, A.; Menand, A. Three-Dimensional Atomic-Scale Imaging of Impurity Segregation to Line Defects. *Science (80-.).* **1999**, *286* (5448), 2317–2319. https://doi.org/10.1126/science.286.5448.2317.

(31) Miller, M. K. Atom Probe Tomography Characterization of Solute Segregation to Dislocations and Interfaces. *J. Mater. Sci.* **2006**, *41* (23), 7808–7813. https://doi.org/10.1007/s10853-006-0518-5.

(32) Usami, S.; Mayama, N.; Toda, K.; Tanaka, A.; Deki, M.; Nitta, S.; Honda, Y.; Amano, H. Direct Evidence of Mg Diffusion through Threading Mixed Dislocations in GaN p-n Diodes and Its Effect on Reverse Leakage Current. *Appl. Phys. Lett.* **2019**, *114* (23), 232105. https://doi.org/10.1063/1.5097767.

(33) Kumar, A.; Uzuhashi, J.; Ohkubo, T.; Tanaka, R.; Takashima, S.; Edo, M.; Hono, K. Atomic-Scale Quantitative Analysis of Implanted Mg in Annealed GaN Layers on Free-Standing GaN Substrates. *J. Appl. Phys.* **2019**, *126* (23), 235704. https://doi.org/10.1063/1.5132345.

(34) Licata, O. G.; Broderick, S.; Rocco, E.; Shahedipour-Sandvik, F.; Mazumder, B. Dopant-Defect Interactions in Mg-Doped GaN via Atom Probe Tomography. *Appl. Phys. Lett.* **2021**, *119* (3), 32102. https://doi.org/10.1063/5.0061153.

(35) Bonef, B.; Shah, R. D.; Mukherjee, K. Fast Diffusion and Segregation along Threading Dislocations in Semiconductor Heterostructures. *Nano Lett.* **2019**, *19* (3), 1428–1436. https://doi.org/10.1021/acs.nanolett.8b03734.

(36) Tomiya, S.; Kanitani, Y.; Tanaka, S.; Ohkubo, T.; Hono, K. Atomic Scale Characterization of GaInN/GaN Multiple Quantum Wells in V-Shaped Pits. *Appl. Phys. Lett.* **2011**, *98* (18), 181904. https://doi.org/10.1063/1.3585118.

(37) Bian, M. Z.; Sasaki, T. T.; Nakata, T.; Yoshida, Y.; Kawabe, N.; Kamado, S.; Hono, K. Bake-Hardenable Mg–Al–Zn–Mn–Ca Sheet Alloy Processed by Twin-Roll Casting. *Acta Mater.* **2018**, *158*, 278–288. https://doi.org/10.1016/j.actamat.2018.07.057.

(38) Nicolas, J.; Assali, S.; Mukherjee, S.; Lotynk, A.; Moutanabbir, O. Dislocation Pipe Diffusion and Solute Segregation During the Growth of Metastable GeSn. *Cryst. Growth Des.* **2020,** *20* (5), 3493–3498. https://doi.org/10.1021/acs.cgd.0c00270

(39) Mukherjee, S.; Assali, S.; Moutanabbir, O. Atomic Pathways of Solute Segregation in the Vicinity of Nanoscale Defects. *Nano Lett.* **2021**, *21* (23), 9882–9888. https://doi.org/10.1021/acs.nanolett.1c02577

(40) Kioseoglou, J. Atomic Scale Modeling of Edge *a*-Type Dislocations in InN. *Phys. Status Solidi Appl. Mater. Sci.* **2013**, *210* (1), 204–208. https://doi.org/10.1002/pssa.201200538.

(41) Legros, M.; Dehm, G.; Arzt, E.; Balk, T. J. Observation of Giant Diffusivity Along Dislocation Cores. *Science (80-.).* **2008**, *319* (5870), 1646–1649. https://doi.org/10.1126/science.1151771.

(42) Garbrecht, M.; Saha, B.; Schroeder, J. L.; Hultman, L.; Sands, T. D. Dislocation-Pipe Diffusion in Nitride Superlattices Observed in Direct Atomic Resolution. *Sci. Rep.* **2017**, *7*, 46092. https://doi.org/10.1038/srep46092.

For Table of Contents Only